



Published in final edited form as:

Neuron. 2016 August 3; 91(3): 602–614. doi:10.1016/j.neuron.2016.07.003.

## Defining preBötzinger Complex rhythm and pattern generating neural microcircuits *in vivo*

Yan Cui<sup>1,2</sup>, Kaiwen Kam<sup>2,†</sup>, David Sherman<sup>2</sup>, Wiktor A. Janczewski<sup>2</sup>, Yu Zheng<sup>1</sup>, and Jack L. Feldman<sup>2,\*</sup>

<sup>1</sup>Department of Physiology, West China School of Preclinical and Forensic Medicine, Sichuan University, Chengdu, Sichuan 610041, People's Republic of China

<sup>2</sup>Department of Neurobiology, David Geffen School of Medicine at UCLA, Los Angeles, CA 90095, USA

### Summary

Normal breathing in rodents requires activity of glutamatergic Dbx1-derived (Dbx1<sup>+</sup>) preBötzinger Complex (preBötC) neurons expressing somatostatin (SST). We combined *in vivo* optogenetic and pharmacological perturbations to elucidate the functional roles of these neurons in breathing. In transgenic adult mice expressing channelrhodopsin (ChR2) in Dbx1<sup>+</sup> neurons, photoresponsive preBötC neurons had preinspiratory or inspiratory firing patterns associated with excitatory effects on burst timing and pattern. In transgenic adult mice expressing ChR2 in SST<sup>+</sup> neurons, photoresponsive preBötC neurons had inspiratory or postinspiratory firing patterns associated with excitatory responses on pattern or inhibitory responses that were largely eliminated by blocking synaptic inhibition within preBötC or by local viral infection limiting ChR2 expression to preBötC SST<sup>+</sup> neurons. We conclude that: i) preinspiratory preBötC Dbx1<sup>+</sup> neurons are rhythmogenic; ii) inspiratory preBötC Dbx1<sup>+</sup> and SST<sup>+</sup> neurons primarily act to pattern respiratory motor output, and; iii) SST<sup>+</sup> neuron-mediated pathways and postsynaptic inhibition within preBötC modulate breathing pattern.

### eTOC Blurp

Cui *et al.* combine *in vivo* optogenetic and pharmacological perturbations to dissect the neural microcircuits controlling breathing and elucidate the functional role of preBöttinger Complex Dbx1<sup>+</sup> and SST<sup>+</sup> neurons that underlie a microcircuit model for respiratory rhythm and pattern generation.

\*Correspondence: Jack L. Feldman, Ph.D. Department of Neurobiology, David Geffen School of Medicine at UCLA, Box 951763, Los Angeles CA 90095-1763, USA, feldman@ucla.edu, Phone: (310) 825-1586, Fax: (310) 825-2224.

†Current address: Department of Cell Biology and Anatomy, Chicago Medical School, Rosalind Franklin University of Medicine and Science, 3333 Green Bay Rd., North Chicago, IL 60064. kaiwen.kam@rosalindfranklin.edu. Phone: (847) 578-8630.

‡This research is done in partial fulfillment of Yan Cui's Ph.D. degree at Sichuan University. All research was done at UCLA.

**Author contributions:** Y.C., W.A.J. and J.L.F. designed the research; Y.C. and D.S. performed the research with help from W.A.J.; Y.C. and K.K. analyzed the data with help from D.S.; Y.C., K.K. and J.L.F. wrote the paper. Y.Z. and W.A.J. commented on an early draft of the paper.

**Publisher's Disclaimer:** This is a PDF file of an unedited manuscript that has been accepted for publication. As a service to our customers we are providing this early version of the manuscript. The manuscript will undergo copyediting, typesetting, and review of the resulting proof before it is published in its final citable form. Please note that during the production process errors may be discovered which could affect the content, and all legal disclaimers that apply to the journal pertain.

## Introduction

The preBötzinger Complex (preBötC) is a heterogeneous medullary population of ~1000–3000 neurons/side that is the presumptive kernel for respiratory rhythm generation in rodents (Feldman et al., 2013; Gray et al., 2001; Tan et al., 2008) and presumably in humans (Benarroch et al., 2003; Schwarzacher et al., 2011). preBötC heterogeneity is reflected in various molecularly-defined subpopulations that may underlie different functions during breathing (Feldman and Kam, 2015; Stornetta et al., 2003; Tan et al., 2012; Winter et al., 2009).

The transcription factor Dbx1 gives rise to neurons throughout the brain, including glutamatergic preBötC neurons necessary for respiratory rhythm generation (Bouvier et al., 2010; Funk et al., 1993; Gray et al., 2010; Wallén-Mackenzie et al., 2006). preBötC Dbx1<sup>+</sup> neurons are strong candidates as generators of inspiratory rhythm (Wang et al., 2014). In rhythmically active slice preparations from neonatal rodents, preBötC Dbx1<sup>+</sup> neurons have a preinspiratory firing pattern, initiating spike activity before the onset of each inspiratory hypoglossal nerve burst, and continue to fire throughout inspiration (Picardo et al., 2013). *In vitro*, a subset of Dbx1<sup>+</sup> neurons are premotoneurons, projecting directly to motoneurons, transmitting bursts of inspiratory activity that ultimately pattern inspiratory muscle contraction (Kam et al., 2013a; Revill et al., 2015; Wang et al., 2014). SST is expressed in a subset of preBötC Dbx1<sup>+</sup> neurons that partially overlap with neurokinin 1 receptor-positive (NK1R<sup>+</sup>) neurons (Gray et al., 2010; Stornetta et al., 2003). In unanesthetized adult rats, targeted, slow (~days) ablation of NK1R<sup>+</sup> preBötC neurons (Gray et al., 2001) results in ataxic breathing patterns during wakefulness and apnea during sleep (McKay et al., 2005) whereas acute (~minutes) silencing of SST<sup>+</sup> preBötC neurons results in persistent apnea (Tan et al., 2008). Together these data indicate that in rodents (*in vitro* and *in vivo*) preBötC Dbx1<sup>+</sup> and SST<sup>+</sup> neurons are critical for generating and patterning rhythmic inspiratory motor nerve bursts that drive breathing movements.

Photostimulation of preBötC neurons expressing Channelrhodopsin-2 (ChR2) driven by the synapsin promoter potently drives inspiratory activity *in vivo* (Alsahafi et al., 2015). However, synapsin is a pan-neuronal promoter that cannot distinguish among different populations of excitatory and inhibitory neurons. Consequently, the preBötC subpopulations responsible for excitation-mediated rhythm and pattern generation (Greer et al., 1991) and for the roles of GABA- and glycine-mediated postsynaptic inhibition in the Breuer-Hering Inflation Reflex (BHIR) (Janczewski et al., 2013), in modulating breathing frequency, in shaping the pattern of respiratory motor output, and in producing apneas essential for such behaviors as swallowing, phonation, and breathholding (Sherman et al., 2015) must still be specified.

The functional role of various preBötC subpopulations can be elucidated by differentially perturbing their excitability, e.g., for inhibitory neurons (Sherman et al., 2015). To determine the *in vivo* roles of preBötC Dbx1<sup>+</sup> and SST<sup>+</sup> neurons in rhythm and pattern generation and deconstruct the related neural microcircuits, we employed Cre/loxP transgenic strategies to express ChR2-tdTomato in Dbx1<sup>+</sup> neurons (Dbx1-ChR2) or SST<sup>+</sup> neurons (SST-ChR2). We also expressed ChR2 in preBötC SST<sup>+</sup> neurons by targeted injection of a Cre-dependent

Chr2 virus into the preBötC of transgenic mice expressing Cre recombinase in SST<sup>+</sup> neurons. We then examined the effects of photostimulation on breathing. We conclude that the preBötC is composed of partially overlapping subpopulations that form functionally distinct rhythm and pattern generating microcircuits. We suggest that: i) the onset of activity in preinspiratory Dbx1<sup>+</sup> neurons initiates each inspiration (Kam et al., 2013a); ii) Dbx1<sup>+</sup> and SST<sup>+</sup> inspiratory neurons primarily act in a patterning role to transmit activity from rhythmogenic preBötC neurons (Revilla et al., 2015; Tan et al., 2010) and ultimately shape inspiratory motoneuronal activity; iii) SST<sup>+</sup> neuron-mediated inhibitory pathways modulate respiratory activity; and iv) postsynaptic inhibition within the preBötC induces apneas, broadens the dynamic range of inspiratory burst amplitude, and stabilizes the rhythm in the presence of significant perturbations, but is not obligatory for rhythmogenesis (Janczewski et al., 2013; Sherman et al., 2015).

## Results

### Selective expression of opsins in Dbx1<sup>+</sup> and SST<sup>+</sup> neurons

We crossed mice expressing Cre recombinase under either the Dbx1 promoter (Dbx1-Cre; Bielle et al., 2005) or SST promoter (Sst-IRES-Cre, abbreviated as SST-Cre; Jackson labs, Stock Number: 013044) with floxed-ChR2-tdTomato mice (Ai27; ChR2(H134R)-tdTomato; Jackson labs, Stock Number: 012567). These crosses resulted in mice expressing ChR2 in Dbx1<sup>+</sup> neurons (Dbx1-Cre;ChR2(H134R)-tdTomato, abbreviated as Dbx1-ChR2) or SST<sup>+</sup> neurons (Sst-IRES-Cre;ChR2(H134R)-tdTomato, abbreviated as SST-ChR2), with tdTomato as a fluorescent reporter. The expression patterns of ChR2 in Dbx1-ChR2 and SST-ChR2 mice were analyzed via SST immunostaining and tdTomato fluorescence.

In brainstems of adult Dbx1-ChR2 mice at the rostrocaudal level of the preBötC, tdTomato fluorescence extended from the area directly lateral to the hypoglossal (XII) motor nucleus to the ventral medullary surface encompassing the intermediate reticular formation (IRt) and the ventral respiratory column (VRC) (Figure 1A), consistent with previous data in newborn mice (Gray, 2013; Ruangkittisakul et al., 2014). tdTomato fluorescence was also present within the spinal trigeminal nucleus, interpolar part (Sp5I) region lateral to IRt (Figure 1A). The nucleus ambiguus (NA) and XII motor nucleus were devoid of tdTomato fluorescence (Figure 1A) as in newborn mice (Gray, 2013; Ruangkittisakul et al., 2014).

Ventral to nucleus ambiguus (NA) (Figure 1A, square segment) were a subset of Dbx1<sup>+</sup> glutamatergic preBötC SST-expressing respiratory neurons (Figures 1B–1C), essential for breathing movements in adult rats (Tan et al., 2008). In the ventrolateral medulla of adult Dbx1-ChR2 (Figures 1A–1C) and SST-ChR2 (Figures 1D and 1F) mice, tdTomato predominately overlapped with the distribution of SST-expressing neurons that demark the preBötC (Stornetta et al., 2003).

### Firing patterns of photoresponsive preBötC neurons in Dbx1-ChR2 and SST-ChR2 mice

We recorded the extracellular firing patterns of respiratory-modulated preBötC neurons in Dbx1-ChR2 and SST-ChR2 adult mice that responded to preBötC photostimulation, which would include neurons directly excited by light and those receiving input from these

neurons. We observed three types of neuronal firing patterns: preinspiratory (pre-I), inspiratory (I), and postinspiratory (post-I) (Figure 2). In Dbx1-ChR2 mice (Figure 2, middle column), in response to bilateral preBötC short pulse photostimulation (SPP; 100–300 ms pulse; 473 nm) at any point in the respiratory cycle, we observed increased firing in all preinspiratory (n=12/12 units in 3 mice) and most inspiratory (n=4/7 units in 3 mice) preBötC neurons, with no responsive postinspiratory (n=0/9 units in 3 mice) preBötC neurons; these results are consistent with the firing patterns of identified preBötC Dbx1<sup>+</sup> neurons *in vitro* (Picardo et al., 2013). In SST-ChR2 mice (Figure 2, right column), all recorded inspiratory (n=5/5 units in 2 mice) and all postinspiratory (n=5/5 units in 2 mice) preBötC neurons, but no preinspiratory (n=0/15 units in 2 mice) preBötC neurons were responsive to bilateral preBötC SPP at any point in the respiratory cycle.

All light-induced increases in firing rate were proportional to laser intensity (Figure S1). Typically, 3–6 mW laser power initiated a burst of action potentials but no motor output, whereas >6 mW could trigger motor output in Dbx1-ChR2 mice (Figure S1). Unless otherwise specified, laser power was set at 7 mW.

### Role of preBötC Dbx1<sup>+</sup> neurons in burst timing and motor output pattern

In Dbx1-ChR2 mice, we examined the role of preBötC Dbx1<sup>+</sup> neurons by photostimulation at different phases of expiration (phase: 0.0–0.8) or inspiration (phase: 0.9–1.0). For stimulation during each phase, we measured genioglossus electromyographic activity (GG<sub>EMG</sub>) and calculated the resultant phase shift (phase shift=perturbed cycle duration/control cycle duration). If a stimulus had no effect, the perturbed cycle duration would equal the control cycle duration, and the phase shift would be 1.0 (see Supplemental Experimental Procedures). No ectopic inspiratory burst could be generated by bilateral preBötC SPP during early expiration or postinspiration (phase: 0.0–0.1; phase shift: 1.0±0.03; P=0.7, n=5). Bilateral preBötC SPP during mid (phase: 0.2–0.7) or late (phase: 0.8) expiration elicited an ectopic inspiratory burst and shifted the respiratory phase (n=5; Figure 3A) without affecting GG<sub>EMG</sub> burst amplitude (P=0.9, n=5), inspiratory duration ( $T_I$ ; P=0.1, n=5), or expiratory duration ( $T_E$ ) of the following cycle (P=1.0, n=5). Bilateral preBötC SPP in early inspiration (phase: 0.9) increased GG<sub>EMG</sub> burst amplitude to 315±32% of control (P=3×10<sup>-5</sup>, n=6; Figure 3B) in the stimulus cycle and decreased GG<sub>EMG</sub> burst amplitude in the following poststimulus cycle to 79±14% of control (P=0.004, n=6; Figure 3B). The strongest phase resetting was at phase 0.3 (phase shift: 0.6±0.03; P<10<sup>-16</sup>, n=5; Figure 3J, red curve). For SPP during expiration in Dbx1-ChR2 mice, the latency between photostimulation onset and ectopic inspiratory burst onset was inversely related to the phase of stimulation, with stimulation at later expiratory phases requiring less time to evoke a response. Bilateral preBötC SPP produced ectopic bursts with delays of: 235±28 ms early in midexpiration (phase: 0.2–0.3; n=5); 131±35 ms in the middle of midexpiration (phase: 0.4–0.6; P=8×10<sup>-4</sup>, n=5), and; 59±29 ms late in midexpiration (phase 0.7; P=0.007, n=5).

The Breuer-Hering inhibitory reflex (BHIR) is a powerful lung inflation-induced, vagus nerve-mediated reflex that results in a sustained apnea mediated by fast synaptic inhibition within the preBötC (Janczewski et al., 2013; Sherman et al., 2015). In Dbx1-ChR2 mice, apnea caused by a prolonged BHIR could be broken by bilateral preBötC SPP. Apnea

induced by a 10 s lung inflation using constant positive air pressure (CPAP; 8 cm H<sub>2</sub>O) in control ranged from 8.8 to 10.1 s ( $9.6 \pm 0.5$  s,  $n=5$ ; Figure 3C, top traces). Bilateral preBötC SPP at  $3.0 \pm 0.8$  s after onset of CPAP induced an inspiratory burst within  $145 \pm 37$  ms of laser onset (Figure 3C, bottom traces;  $n=5$ ), indicating that acute activation of this neuronal subpopulation can trigger inspiration despite inhibitory effects of vagal pulmonary afferents.

Bilateral preBötC long pulse photostimulation (LPP; 4–10 s pulse; 473 nm) increased GG<sub>EMG</sub> burst amplitude to  $402 \pm 58\%$  of control in the stimulus cycle ( $P=4 \times 10^{-7}$ ,  $n=5$ ; Figure 3D), but did not significantly change the amplitude in poststimulus cycles ( $P=0.07$ ,  $n=5$ ). Breathing frequency ( $f$ ) increased to  $120 \pm 6\%$  of control when baseline  $f < 100$  breaths per minute (bpm;  $83 \pm 9$  bpm,  $P=0.003$ ,  $n=7$ ) due to a decrease in  $T_E$  to  $83 \pm 7\%$  of control ( $P=0.01$ ,  $n=7$ ), with no significant change in  $T_I$  ( $P=0.3$ ,  $n=7$ ). At higher baseline  $f > 100$  bpm ( $112 \pm 5$  bpm,  $n=5$ ),  $f$  did not change ( $P=0.5$ ,  $n=5$ ). In no cases were apneas induced ( $n=5$ ). During bilateral preBötC LPP (5 mW) in Dbx1-ChR2 mice, preinspiratory neurons continued their firing except for a refractory period of  $\sim 0.3$  s that followed endogenous bursts ( $n=4$  units in 3 mice; Figure 3E, top traces). Postinspiratory neurons were not responsive to photostimulation ( $n=4$  units in 3 mice; Figure 3E, bottom traces).

Thus, preBötC photostimulation in Dbx1-ChR2 mice can evoke ectopic inspiratory bursts during the expiratory phase or during the apnea induced by the BHIR, as well as increase GG<sub>EMG</sub> when delivered during an ongoing inspiratory cycle. We suggest that the effects on burst timing and output pattern in response to preBötC photostimulation in Dbx1-ChR2 mice result from photostimulation-induced firing of Dbx1<sup>+</sup> preinspiratory and inspiratory neurons.

## Role of preBötC SST<sup>+</sup> neurons and SST<sup>+</sup> neuron-mediated pathways in pattern generation

**Effects of preBötC photostimulation in SST-ChR2 mice on burst timing and motor output pattern**—In SST-ChR2 mice, bilateral preBötC SPP during early inspiration had presumptively excitatory effects on inspiratory motor output pattern, increasing GG<sub>EMG</sub> burst amplitude to  $275 \pm 43\%$  compared to control ( $P=4 \times 10^{-5}$ ,  $n=6$ ; Figure 3G) in the stimulus cycle and decreasing GG<sub>EMG</sub> burst amplitude in the following cycle to  $83 \pm 13\%$  of control ( $P=0.007$ ,  $n=6$ ). In contrast to these effects, bilateral preBötC SPP during mid (phase: 0.3–0.7) or late (phase: 0.8) expiration significantly delayed the onset of the next inspiration and did not trigger ectopic inspiratory bursts, unlike in Dbx1-ChR2 mice (Figure 3F, compare to Figure 3A). The longest delay was at phase 0.7 (phase shift:  $1.4 \pm 0.03$ ;  $P < 10^{-16}$ ,  $n=6$ ; Figure 3J, blue curve);  $T_E$  of the next cycle was not lengthened ( $P=0.4$ ,  $n=6$ ).

Bilateral preBötC LPP in SST-ChR2 mice initiated in early inspiration triggered a single augmented burst that in GG<sub>EMG</sub> was  $257 \pm 31\%$  larger than control ( $P=8 \times 10^{-6}$ ,  $n=4$ ; Figure 3H), followed by apnea for the remaining stimulation (Figure 3H). With 4 s LPP, the length of stimulation-induced apnea was  $3.8 \pm 0.1$  s ( $n=4$ ; Figure 3H), and poststimulation  $f$  was not significantly different from prestimulus  $f$  ( $P=1.0$ ,  $n=4$ ). Preinspiratory neurons were silenced ( $n=12$  units in 2 mice; Figure 3I), while postinspiratory neurons ( $n=5$  units in 2 mice; Figure 3I) fired throughout the photostimulation-induced apnea. We suggest that the excitatory effect on motor output pattern in response to preBötC photostimulation in SST-ChR2 mice

results from the photostimulation-induced firing of SST<sup>+</sup> inspiratory neurons, while an inhibitory pathway may be activated by photostimulation-induced firing of preBötC SST<sup>+</sup> postinspiratory neurons, or by activation of postinspiratory neurons postsynaptic to preBötC excitatory SST<sup>+</sup> neurons.

**SST antagonism does not eliminate apnea induced by bilateral preBötC LPP in SST-ChR2 mice**—In SST-ChR2 mice, preinspiratory neurons were silenced during photostimulation-induced apnea, suggesting strong activation of an inhibitory pathway affecting rhythmogenic neurons. We first investigated whether this response was due to the release of SST within the preBötC (Martel et al., 2012).

In SST-ChR2 mice, bilateral injection into preBötC of the broad spectrum SST receptor antagonist cyclosomatostatin (CSST) increased GG<sub>EMG</sub> burst amplitude to 374±56% of control (P=0.007, n=4), decreased *f* to 54±10% of control (P=0.0004, n=4; Figure 4A1), increased *T<sub>E</sub>* to 226±52% of control (P=0.01, n=4; Figure 4A1) and did not change *T<sub>I</sub>* significantly (P=0.2, n=4; Figure 4A1). With 4 s LPP, the length of photostimulation-induced apnea was 4.0±0.04 s (n=4; Figure 4A3), i.e., there was no significant effect of CSST administration on the apnea elicited by bilateral preBötC LPP (Figure 4A2). Poststimulation *f* did not change significantly (P=0.8, n=4). We confirmed that CSST effectively blocked SST receptors, as respiratory responses induced by SST administration into the preBötC (where *f* decreased to 29±1% of control) were fully antagonized by CSST (n=4; Figure S2).

**GABA and/or glycine mediate the inhibitory effect of preBötC photostimulation in SST-ChR2 mice**—As the apnea induced by bilateral preBötC LPP in SST-ChR2 mice was not mediated by the local release of SST, we investigated the involvement of inhibition mediated by local release within preBötC of GABA and/or glycine from the terminals of GABAergic SST<sup>+</sup> neurons with somas either inside or outside the preBötC (Wei et al., 2012) and/or GABAergic/glycinergic neurons postsynaptic to glutamatergic SST<sup>+</sup> neurons.

In SST-ChR2 mice, after bilateral injection of the GABA<sub>A</sub> and glycine receptor antagonists bicuculline and strychnine (B+S) into preBötC, bilateral preBötC LPP no longer produced apnea or prolongation of *T<sub>E</sub>* (P=0.4, n=4; Figure 4B2, compare with Figures 3H and 4A2) and did not change GG<sub>EMG</sub> burst amplitude (P=0.4, n=4), *f* (P=0.2, n=4) or *T<sub>I</sub>* (P=0.8, n=4) compared to controls, suggesting that the photostimulation-induced apnea was mediated by local release within preBötC of GABA and/or glycine. In SST-ChR2 mice after B+S injection, bilateral preBötC SPP during mid (phase: 0.2–0.7) or late (phase: 0.8) expiration produced ectopic inspiratory bursts, altered the respiratory phase (n=6; Figure 4B1), but did not change the subsequent *T<sub>E</sub>* (P=0.9, n=6). The strongest phase resetting was at phase 0.2 (shift to 0.4±0.02; P<10<sup>-16</sup>, n=6; Figure 4C, light blue curve), while no ectopic inspiratory burst could be generated in early expiration (phase 0.0–0.1, shift to 1.0±0.03; P=0.3, n=6). These data are similar to the effects produced by bilateral preBötC SPP during mid or late expiration in Dbx1-ChR2 mice (Figure 3A), indicating that local inhibition is not involved in the initiation of ectopic inspiratory bursts following preBötC photostimulation in SST-ChR2 mice.



**Excitatory role for SST<sup>+</sup> glutamatergic preBötC neurons in pattern generation and illumination of a SST-mediated inhibitory pathway within preBötC**—To determine whether separate SST<sup>+</sup> subpopulations mediate the differential excitatory and inhibitory effects of photostimulation in SST-ChR2 mice, we bilaterally injected SST-Cre mice with Cre-dependent ChR2-eYFP virus into preBötC, restricting ChR2 expression to preBötC SST<sup>+</sup> neurons. ChR2-eYFP expression was detectable in preBötC neurons 4 weeks after viral injection. The peak density of transfected neurons was caudal to the facial nucleus (VII) by 300–450  $\mu\text{m}$  and ventral to the compact NA (Figures 5A and 5B). Within the preBötC, SST-positive cells and small fusiform NK1R<sup>+</sup> cells were immunoreactive for eYFP (Figures 5C and 5D).

In virally transfected SST-Cre mice, bilateral preBötC SPP in early inspiration increased the  $\text{GG}_{\text{EMG}}$  burst amplitude to  $212 \pm 33\%$  of control ( $P=0.003$ ,  $n=4$ ; Figure 5E), consistent with the effect of bilateral preBötC SPP in SST-ChR2 mice (Figure 3G). Interestingly, bilateral preBötC SPP during midexpiration (phase: 0.2–0.7) was now able to generate ectopic inspiratory bursts, similar to the effects produced by bilateral preBötC SPP in Dbx1-ChR2 mice or in SST-ChR2 mice after B+S injection (Figure 5F, compare with Figures 3A and 4B1), with the strongest phase resetting at phase 0.3 (phase shift:  $0.6 \pm 0.03$ ;  $P < 10^{-16}$ ,  $n=4$ ; Figure 5G). No ectopic inspiratory bursts could be generated by bilateral preBötC SPP during early expiration (phase: 0.0–0.1, shift to  $1.0 \pm 0.02$ ;  $P=1$ ,  $n=4$ ). In addition, the apnea caused by BHIR could be broken by bilateral preBötC SPP. While apneas induced by 10 s lung inflation in control in virally transfected SST-Cre mice ranged from 8.4 to 10.0 s ( $9.2 \pm 0.8$  s,  $n=3$ ; Figure 5H, top traces), multiple bilateral preBötC SPPs with delay times of  $2.1 \pm 0.5$  s between pulses induced a breath with each individual pulse at a  $91 \pm 18$  ms delay from photostimulation onset ( $n=3$ ; Figure 5H, bottom traces). Thus, when afferent inhibitory inputs arising from SST<sup>+</sup> neurons outside the preBötC are eliminated, stimulating preBötC SST<sup>+</sup> neurons can generate ectopic inspiratory bursts.

Bilateral preBötC LPP in virally transfected SST-Cre mice did not produce apnea but decreased  $f$  to  $61 \pm 12\%$  of control ( $P=0.0003$ ,  $n=4$ ), increased  $T_E$  to  $189 \pm 48\%$  of control ( $P=0.004$ ,  $n=4$ ) and did not change  $T_I$  ( $P=0.7$ ,  $n=4$ ; Figure 5I). This response differed from bilateral preBötC LPP after B+S injection in transgenic SST-ChR2 mice where there was no change in  $f$  (Figures 4B2–4B3); this suggests that photostimulation activated an SST-mediated inhibitory pathway within the preBötC to increase  $T_E$ . To test if the remaining inhibitory effect was mediated by GABA and/or glycine, we repeated the photostimulation in the presence of B+S. After B+S injection, bilateral preBötC LPP no longer decreased  $f$  ( $P=0.8$ ,  $n=4$ ; Figure 5J) and did not induce significant changes in  $T_E$  ( $P=0.5$ ,  $n=4$ ) or  $T_I$  ( $P=0.9$ ,  $n=4$ ).

### **Role of fast inhibitory synaptic transmission in the preBötC in rhythm and pattern generation**

The excitatory effects of SST<sup>+</sup> photostimulation were largely masked by the release of GABA and/or glycine until we blocked the inhibition pharmacologically, suggesting that inhibition from SST<sup>+</sup> and other sources normally plays a powerful role in modulating rhythm and pattern generation. To further explore the endogenous tonic and phasic role of

inhibitory inputs into the preBötC, we characterized the effects of B+S in preBötC on breathing in adult mice under control (baseline) conditions and with preBötC photostimulation.

### **Effects of blockade of fast inhibitory synaptic transmission in wild-type mice**

—Consistent with previous data in rats (Janczewski et al., 2013), breathing persisted when B+S were injected bilaterally into the preBötC of adult mice with intact vagus nerves. Relative to control values,  $f$  decreased to  $38\pm 1\%$  ( $P=0.0001$ ,  $n=5$ ),  $T_I$  increased to  $142\pm 15\%$  ( $P=0.03$ ,  $n=5$ ), and  $T_E$  increased to  $305\pm 17\%$  ( $P=0.0001$ ,  $n=5$ ; Figures 6A and 6B). B+S also affected GG<sub>EMG</sub> burst shape (Figure 6A). GG<sub>EMG</sub> burst amplitude increased to  $490\pm 26\%$  ( $P=10^{-5}$ ,  $n=5$ ; Figure 6B), and tidal volume ( $V_T$ ) increased to  $309\pm 44\%$  ( $P=10^{-5}$ ,  $n=5$ ; Figure 6B) of control. Apnea induced by a 10 s lung inflation ( $T_{E-INT}$ ) before B+S injection, i.e., control, ranged from 8.8 to 10.1 s ( $9.8\pm 0.5$  s,  $n=5$ ), and the strength of the BHIR [SBHIR;  $(T_{E-INT}/T_{E-CON})-1$ ,  $T_{E-INT}$ : duration of the resultant inflation-induced apnea,  $T_{E-CON}$ : expiratory duration during the control period; see Supplemental Experimental Procedures] (Janczewski et al., 2013) ranged from 14.6 to 16.7 ( $15.8\pm 0.7$ ,  $n=5$ ; Figure 6C). After bilateral B+S injection, the BHIR was nearly eliminated:  $T_{E-INT}$  was reduced to  $2.4\pm 0.6$  s (range: 1.5 to 3.0 s), which was  $24.3\pm 5.4\%$  of its control value ( $P=5\times 10^{-8}$ ,  $n=5$ ), and SBHIR was  $0.05\pm 0.07$  (range:  $-0.05$  to 0.13), which was only  $0.3\pm 0.5\%$  ( $P=1\times 10^{-6}$ ,  $n=5$ ) of its control value (Figure 6C). This result was comparable to the effect of blocking pulmonary stretch receptors (Davies et al., 1978; Janczewski et al., 2013). Loss of the BHIR serves as a positive control for the effectiveness of B+S in blocking postsynaptic inhibition in preBötC, q.v., (Janczewski et al., 2013).

### **Effects of blockade of fast inhibitory synaptic transmission in the preBötC on rhythmogenesis**

—In Dbx1-ChR2 mice, B+S enhanced the effects of bilateral preBötC photostimulation. After B+S injection, bilateral preBötC SPP during mid (phase: 0.2–0.7) or late (phase: 0.8) expiration elicited an ectopic inspiratory burst and shifted respiratory phase ( $n=5$ , Figure 6D1), with the strongest shift at phase 0.2 (shift to  $0.4\pm 0.03$ ;  $P<10^{-16}$ ,  $n=5$ ; Figure 6E, pink curve). These phase advance effects were always stronger in B+S (Figure 6E, pink curve) compared to control conditions (Figure 6E, dark red curve;  $P=3\times 10^{-5}$ ,  $n=5$ ).

In B+S, bilateral preBötC LPP in Dbx1-ChR2 mice increased  $f$  to  $200\pm 27\%$  of control ( $P=0.0002$ ,  $n=6$ ; Figure 6D2).  $T_I$  did not change significantly ( $P=0.2$ ,  $n=6$ ), and  $T_E$  decreased to  $49\pm 9\%$  of control ( $P=5\times 10^{-5}$ ,  $n=6$ ). The increase in  $f$  caused by bilateral preBötC LPP was significantly greater after B+S injection ( $P=0.0007$ ,  $n=6$ ; Figure 6D3) and produced irregular bursts, i.e., doublets, which could be manifestations of sigh behavior ( $n=6$ , Figure S3; Kam et al., 2013a; Li et al., 2016).

Thus, after blockade of fast inhibitory synaptic transmission, the excitatory effects of photostimulation of preBötC Dbx1<sup>+</sup> neurons on rhythm were enhanced. We suggest that the responsiveness of preBötC rhythmogenic neurons to excitatory inputs is constrained by tonic and/or phasic postsynaptic inhibition at rest.

### **Effects of blockade of fast inhibitory synaptic transmission in the preBötC on pattern generation**

—In Dbx1-ChR2 ( $P=0.9$ ,  $n=6$ ) or SST-ChR2 ( $P=0.4$ ,  $n=6$ ) mice after



B+S injection, bilateral preBötC SPP in early inspiration had no further effect on increasing  $GG_{EMG}$  burst amplitude (Figure 7A). As B+S effectively eliminate the influence of inhibitory vagal pulmonary afferents, we tested the effect of photostimulation on  $GG_{EMG}$  burst amplitude in vagotomized Chr2 mice. In Dbx1-ChR2 ( $P=0.7$ ,  $n=4$ ) or SST-ChR2 ( $P=0.8$ ,  $n=4$ ) vagotomized mice, bilateral preBötC SPP in early inspiration also had no further effect on augmenting  $GG_{EMG}$  burst amplitude (Figure 7B). In the presence of B+S in Dbx1-ChR2 mice, bilateral preBötC LPP slightly decreased  $GG_{EMG}$  burst amplitude to  $87\pm 3\%$  of control ( $P=0.003$ ,  $n=5$ ; Figure 7C). In Dbx1-ChR2 vagotomized mice, bilateral preBötC LPP also did not increase  $GG_{EMG}$  burst amplitude ( $P=0.8$ ,  $n=4$ ; Figure 7C). Thus, in Dbx1-ChR2 or SST-ChR2 mice, after either B+S injection or vagotomy bilateral preBötC photostimulation (SPP or LPP) of preBötC neurons was unable to further increase  $GG_{EMG}$  burst amplitude.

We hypothesized that the inability to increase  $GG_{EMG}$  burst amplitude following B+S injection or vagotomy was due to these manipulations maximally activating  $GG_{EMG}$ . We therefore tested whether  $GG_{EMG}$  burst amplitude in B+S could increase further in response to increased chemical drive induced by hypercapnia (Figure 7D) or hypoxia (Figure 7E) in adult mice with intact vagus nerves. Before B+S injection, relative to control, increasing  $CO_2$  with an inspired gas mixture of 5%  $CO_2$  in air (5%  $CO_2$ , 21%  $O_2$ , 74%  $N_2$ ) increased  $GG_{EMG}$  burst amplitude to  $196\pm 23\%$  ( $P=0.005$ ,  $n=4$ ), increased  $f$  to  $127\pm 4\%$  ( $P=0.005$ ,  $n=4$ ), decreased  $T_E$  to  $75\pm 2\%$  ( $P=0.001$ ,  $n=4$ ), and did not significantly change  $T_I$  ( $P=0.2$ ,  $n=4$ ; Figure 7D). In B+S, adding 5%  $CO_2$  to the inspired gas mixture did not change  $GG_{EMG}$  burst amplitude ( $P=0.8$ ,  $n=4$ ; Figure 7D) but increased  $f$  to  $144\pm 25\%$  of control ( $P=0.008$ ,  $n=4$ ) due to shortening of  $T_E$  to  $66\pm 13\%$  of control ( $P=0.01$ ,  $n=4$ ). Reducing  $O_2$  to 8% of the inspired gas mixture (8%  $O_2$  and 92%  $N_2$ ) relative to control, increased  $GG_{EMG}$  burst amplitude to  $168\pm 34\%$  ( $P=0.002$ ,  $n=4$ ; Figure 7E), increased  $f$  to  $139\pm 20$  ( $P=0.009$ ,  $n=4$ ), decreased  $T_E$  to  $62\pm 16\%$  ( $P=0.007$ ,  $n=4$ ), but did not significantly change  $T_I$  ( $P=0.4$ ,  $n=4$ ). However, with B+S, 8%  $O_2$  also had no significant effect on the  $GG_{EMG}$  burst amplitude ( $P=0.9$ ,  $n=4$ ; Figure 7E), though  $f$  increased to  $161\pm 21\%$  of control ( $P=0.002$ ,  $n=4$ ) due to a decrease in  $T_E$  to  $60\pm 12\%$  of control ( $P=0.02$ ,  $n=4$ );  $T_I$  did not change significantly ( $P=1.0$ ,  $n=4$ ). Thus, upon B+S injection in the preBötC,  $GG_{EMG}$  burst amplitude cannot be further increased with hypercapnia or hypoxia.

Thus, inhibitory inputs onto preBötC pattern generating neurons decreased  $GG_{EMG}$  burst amplitude below maximum value when breathing room air at rest; when inhibition was blocked, burst amplitude was maximized, so that photostimulation of excitatory preBötC neurons was unable to further increase peak  $GG_{EMG}$  amplitude.

## Discussion

The preBötC is a heterogeneous neuronal population critical for respiratory rhythm and pattern generation, and much remains unknown about the role of different molecularly-defined subclasses of preBötC neurons and the related neural microcircuits. The homeobox gene *Dbx1* controls the fate of glutamatergic interneurons required for preBötC development that likely include respiratory rhythmogenic neurons (Bouvier et al., 2010; Gray et al., 2010; Picardo et al., 2013). ~15% of preBötC *Dbx1*<sup>+</sup> neurons are preBötC SST<sup>+</sup> neurons,

necessary for normal breathing in anesthetized or awake adult rats (Gray et al., 2010; Tan et al., 2008). We combined an optogenetic approach with pharmacological perturbation to deconstruct the preBötC neural microcircuit *in vivo* and demonstrated anatomically overlapping but functionally distinct rhythm and pattern generating preBötC microcircuits.

### preBötC rhythmogenic microcircuit (Figures 8 and S4)

We postulated that preBötC burst generation is a sequential process initiated by a low amplitude rhythmogenic preinspiratory component that triggers a high amplitude (pattern generating) inspiratory burst (Feldman and Kam, 2015; Kam et al., 2013a). Here, we propose that preinspiratory Dbx1<sup>+</sup> neurons (Figure 8, Pre-I Dbx1<sup>+</sup>Glu<sup>+</sup>) are an essential element of the rhythmogenic microcircuit that determines timing, i.e., onset of each inspiratory phase. In Dbx1-ChR2 mice, bilateral preBötC SPP during expiration excited all (recorded) preBötC preinspiratory neurons. Although *in vivo* extracellular recording cannot distinguish between neurons directly expressing ChR2 and those postsynaptic to ChR2-expressing neurons, these photoresponsive preinspiratory preBötC neurons *in vivo* likely correspond to photoresponsive preinspiratory preBötC Dbx1<sup>+</sup> neurons that were directly excited *in vitro* (Kottick and Del Negro, 2015). Additionally, in Dbx1-ChR2 mice, preBötC photostimulation had excitatory effects on inspiratory burst timing as: i) bilateral preBötC SPP during mid- or late-expiration generated ectopic bursts that were phase-shifted inspiratory bursts and ii) bilateral preBötC LPP increased *f*. Although preinspiratory neurons started firing with the onset of photostimulation, the onset of evoked ectopic inspiratory motor nerve bursts was delayed ~100 ms, equivalent to the duration of their control period preinspiratory activity and similar to the delay to onset of evoked, ectopic inspiratory motor nerve bursts *in vitro* when four to nine inspiratory-modulated preBötC neurons are photostimulated during the expiratory phase (Kam et al., 2013b).

### preBötC pattern generating microcircuit (Figures 8 and S4)

In Dbx1-ChR2 mice, preBötC photostimulation excited preBötC inspiratory neurons (Figure 8, I Dbx1<sup>+</sup>Glu<sup>+</sup>) and had excitatory effects on motor output pattern, as an augmented inspiratory burst was triggered by bilateral preBötC SPP in early inspiration or by bilateral preBötC LPP. Indeed, a subpopulation of Dbx1<sup>+</sup> neurons has intrinsic membrane properties and premotoneuronal axonal projections consistent with a patterning function (Picardo et al., 2013; Revill et al., 2015; Wang et al., 2014). In SST-ChR2 mice, bilateral preBötC SPP excited inspiratory preBötC neurons (Figure 8, I SST<sup>+</sup>Glu<sup>+</sup>). Bilateral preBötC SPP in SST-ChR2 or in virus transfected SST-Cre mice elicited an augmented inspiratory burst in early inspiration, suggesting a pattern generating role of preBötC SST<sup>+</sup> inspiratory neurons. Bilateral preBötC SPP could elicit ectopic inspiratory bursts in SST-ChR2 mice after B+S injection or in virus transfected SST-Cre mice before B+S injection or during BHIR. We propose that when sufficiently stimulated, preBötC SST<sup>+</sup> inspiratory neurons can initiate ectopic inspiratory bursts by rapidly triggering high amplitude bursts, that in turn activate their projections to downstream ventral respiratory group (VRG) premotor neurons (Kam et al., 2013a; Tan et al., 2010). We suggest that preBötC SST<sup>+</sup> and Dbx1<sup>+</sup> inspiratory neurons, along with preinspiratory Dbx1<sup>+</sup> neurons firing during inspiration, contribute to a pattern generating microcircuit, where SST<sup>+</sup> inspiratory neurons are Dbx1<sup>+</sup> and are a subset of the Dbx1 population; at this point, we cannot exclude the possibility that SST<sup>+</sup> post-inspiratory

neurons are a separate non-Dbx1 population (see below) (Gray et al., 2010; Revill et al., 2015).

These results are consistent with our current models of preBötC rhythm generation in which (a subset of) recurrently connected, preinspiratory, glutamatergic preBötC Dbx1<sup>+</sup> neurons generate low level burstlets that (normally) trigger, within this preinspiratory Dbx1<sup>+</sup> subpopulation as well as in inspiratory Dbx1<sup>+</sup>/SST<sup>+</sup> subpopulations, the collective, high amplitude bursts that drive premotoneuronal and, ultimately, motoneuronal activity (Feldman and Kam, 2015; Kam et al., 2013a; Kam et al., 2013b).

### SST<sup>+</sup> neuron-mediated inhibition (Figures 8 and S4)

In SST-ChR2 mice, bilateral preBötC LPP induced apnea, silenced all preinspiratory neurons, and activated postinspiratory neurons; this apnea was eliminated by preBötC inhibitory blockade (via bilateral preBötC injection of B+S) or in virus transfected SST-Cre mice (where ChR2 expression outside the preBötC was greatly reduced or eliminated. Note: The differences between transgenic SST-ChR2 mice and virus transfected SST-Cre mice suggest caution in interpretation of optogenetic data obtained solely from transgenic SST mice, q.v., Koizumi et al., 2016). These predominantly inhibitory responses affecting preBötC preinspiratory neurons in SST-ChR2 mice thus appear mediated by GABA and/or glycine, and could largely be due to activation of GABAergic SST<sup>+</sup> terminals (Figure 8, SST<sup>+</sup>GAD<sup>+</sup>/GlyT2<sup>+</sup>) from sources outside the preBötC (Figure 8, P1), such as the nucleus of the solitary tract (NTS) or the parabrachial nuclei (PB) that contain SST<sup>+</sup> neurons with inhibitory inputs onto preBötC neurons (Figure 8, PB/NTS) (Epelbaum et al., 1994; Johansson et al., 1984; Wei et al., 2012). Besides GABAergic SST<sup>+</sup> afferents outside the preBötC (Figure 8, SST<sup>+</sup>GAD<sup>+</sup>/GlyT2<sup>+</sup>, P1), a weaker inhibitory pathway within preBötC, revealed by the decreased *f* following photostimulation in virus transfected SST-Cre mice, may also exist, consisting of previously unidentified GABAergic and/or glycinergic preBötC postinspiratory SST<sup>+</sup> neurons (Figure 8, Post-I SST<sup>+</sup>GAD<sup>+</sup>/GlyT2<sup>+</sup>, P2) or non-SST<sup>+</sup> glycinergic and/or GABAergic postinspiratory neurons (Figure 8, Post-I GAD<sup>+</sup>/GlyT2<sup>+</sup>, P3) that are postsynaptic to glutamatergic SST<sup>+</sup> neurons (Figure 8, I SST<sup>+</sup>Glu<sup>+</sup>). Since effective doses of the SST antagonist CSST did not abolish these effects, SST release did not mediate this inhibition. However, SST released within preBötC (from indeterminate sources) may play an inhibitory role under certain physiological or pathophysiological conditions (Llona and Eugenin, 2005).

### Roles of inhibition in respiratory rhythm and pattern generation

Our observations of the effects of blocking inhibition within the preBötC confirmed that the preBötC can generate rhythmic inspiratory bursts in the absence of postsynaptic inhibition (Janczewski et al., 2013; Sherman et al., 2015). However, inhibition modulates both respiratory rhythm and pattern in several ways. i) Inhibition within preBötC can play an important role in control of airway muscles including the genioglossus, as upper airway muscle activity is suppressed by the BHIR (Kuna, 1986). After blocking inhibition within preBötC, we observed strong activation of GG<sub>EMG</sub> activity. ii) Inhibition can powerfully interrupt inspiratory rhythmogenesis. Bilateral preBötC SPP and LPP of presumptive SST<sup>+</sup> inhibitory inputs increased  $T_E$  and induced a prolonged apnea, respectively, akin to apneas

induced by the BHIR or prolonged photostimulation of Chr2-expressing preBötC GlyT2<sup>+</sup> neurons (Janczewski et al., 2013; Sherman et al., 2015). iii) Inspiratory rhythm is more labile to perturbations after blocking inhibition. In Dbx1-ChR2 mice after blocking inhibition, preBötC SPP during mid or late expiration produced a stronger phase resetting, and preBötC LPP produced a greater increase in  $f$  and irregular bursts, i.e., doublets that we postulate are sighs (Kam et al., 2013a; Li et al., 2016). Tonic or phasic postsynaptic inhibitory inputs may stabilize preBötC neuron membrane potential, and thereby reduce or prevent rhythmic fluctuations induced by spurious excitatory input. iv) Inhibition may increase the dynamic range of peak inspiratory burst amplitude by keeping it well below maximum value. Thus, when preBötC inhibition is greatly reduced, motor burst amplitude appears maximal and cannot increase further to compensate for increased demand, restricting the dynamic range of inspiratory output. We suggest this effect is due to tonic or phasic inhibition at rest of preBötC pattern generating neurons. Therefore, inhibition, while not necessary for inspiratory rhythmogenesis, appears critical for shaping breathing movements and behavior by mediating apneas, increasing temporal stability, and permitting patterning lability.

In summary, we combined an optogenetic approach with pharmacological perturbation to dissect the neural microcircuits controlling breathing and to elucidate the functional role of preBötC Dbx1<sup>+</sup> and SST<sup>+</sup> neurons *in vivo*. We suggest a concatenated preBötC microcircuit in which preinspiratory Dbx1<sup>+</sup> neurons are essential elements of the inspiratory rhythmogenic kernel that activates inspiratory Dbx1<sup>+</sup> and SST<sup>+</sup> neurons that primarily serve a non-rhythmogenic role by shaping the respiratory output pattern. Convolved with the rhythm and pattern generating functions of these excitatory neurons is postsynaptic inhibition within the preBötC that mediates apneas, broadens the dynamic range of inspiratory burst amplitude, and stabilizes the rhythm in the presence of perturbations. These findings have significant implications for our understanding of the functional roles of distinct preBötC neuronal phenotypes in generation of respiratory rhythm and provide the foundation for highly constrained and testable models with the potential to provide a clear understanding of breathing.

## Experimental Procedures

Animal use and experimental protocols were approved by the University of California, Los Angeles, Animal Research Committee.

## Transgenic mice and Viral Vector

Chr2(H134R)-tdTomato mice were crossed to Dbx1-Cre and SST-Cre mice. For viral transfection of Chr2, SST-Cre mice were infected with *AAV2/1-Efla-DIO-ChR2-eYFP*. See detailed Supplemental Experimental Procedures.

## Photostimulation and Reset Analysis

Once the ventral brainstem surface was exposed (See Supplemental Experimental Procedures), a 473 nm laser connected to a branching fiber patch cord with two 200  $\mu$ m

diameter fibers were placed in soft contact with the ventral surface, 0.15 mm caudal to the hypoglossal canal and 1.2 mm lateral to the midline (Figure 1E), ~250  $\mu\text{m}$  ventral to the preBötC. Photostimulation parameters and reset analysis are provided in the Supplemental Experimental Procedures.

## Unit recording and Pharmacological injection

Unit recordings were done in Dbx1-ChR2 and SST-ChR2 mice. Bicuculline methiodide and strychnine hydrochloride were injected together (Figure S5; B+S, 250  $\mu\text{M}$  each, 50–60 nl/side) to block fast inhibitory synaptic transmission. Cyclosomatostatin (125  $\mu\text{M}$ , 50–60 nl/side; Sigma-Aldrich) was used as a broad spectrum somatostatin receptor antagonist. The protocols for unit recording, pharmacological injection and histology are provided in the Supplemental Experimental Procedures.

## Data analysis and statistics

Unpaired t-tests were used to determine statistical significance of changes before and after photostimulation or pharmacological injections. For statistical comparisons of more than two groups, repeated-measures (RM) ANOVAs were performed. For one-way and two-way RM ANOVAs, post hoc significance for pairwise-comparisons was analyzed using Holm-Sidak method. Significance was set at  $P < 0.05$ . Data are shown as mean  $\pm$  SD. See detailed Supplemental Experimental Procedures.

## Supplementary Material

Refer to Web version on PubMed Central for supplementary material.

## Acknowledgments

The authors thank Grace Li for excellent technical work and Drs. Xuesi M. Shao, Jason Worrell and Robert Huckstepp for thoughtful discussion and Dr. Christopher DeI Negro for additional comments on the revised manuscript. This work was supported by National Institutes of Health grants NS07221, NS58280 and China Scholarship Council (CSC) Joint-Training Program.

## References

- Alsahafi Z, Dickson CT, Pagliardini S. Optogenetic excitation of preBotzinger complex neurons potently drives inspiratory activity in vivo. *The Journal of physiology*. 2015; 593:3673–3692. [PubMed: 26010654]
- Benarroch EE, Schmeichel AM, Low PA, Parisi JE. Depletion of ventromedullary NK-1 receptor-immunoreactive neurons in multiple system atrophy. *Brain : a journal of neurology*. 2003; 126:2183–2190. [PubMed: 12902309]
- Bielle F, Griveau A, Narboux-Neme N, Vigneau S, Sigrist M, Arber S, Wassef M, Pierani A. Multiple origins of Cajal-Retzius cells at the borders of the developing pallium. *Nature neuroscience*. 2005; 8:1002–1012. [PubMed: 16041369]
- Bouvier J, Thoby-Brisson M, Renier N, Dubreuil V, Ericson J, Champagnat J, Pierani A, Chedotal A, Fortin G. Hindbrain interneurons and axon guidance signaling critical for breathing. *Nature neuroscience*. 2010; 13:1066–1074. [PubMed: 20680010]
- Davies A, Dixon M, Callanan D, Huszczuk A, Widdicombe JG, Wise JC. Lung reflexes in rabbits during pulmonary stretch receptor block by sulphur dioxide. *Respiration physiology*. 1978; 34:83–101. [PubMed: 705078]

- Epelbaum J, Dournaud P, Fodor M, Viollet C. The neurobiology of somatostatin. *Critical reviews in neurobiology*. 1994; 8:25–44. [PubMed: 7907281]
- Feldman JL, Del Negro CA, Gray PA. Understanding the rhythm of breathing: so near, yet so far. *Annual review of physiology*. 2013; 75:423–452.
- Feldman JL, Kam K. Facing the challenge of mammalian neural microcircuits: taking a few breaths may help. *The Journal of physiology*. 2015; 593:3–23. [PubMed: 25556783]
- Funk GD, Smith JC, Feldman JL. Generation and transmission of respiratory oscillations in medullary slices: role of excitatory amino acids. *Journal of neurophysiology*. 1993; 70:1497–1515. [PubMed: 8283211]
- Gray PA, Hayes JA, Ling GY, Llona I, Tupal S, Picardo MC, Ross SE, Hirata T, Corbin JG, Eugenin J, et al. Developmental origin of preBotzinger complex respiratory neurons. *The Journal of neuroscience : the official journal of the Society for Neuroscience*. 2010; 30:14883–14895. [PubMed: 21048147]
- Gray PA, Janczewski WA, Mellen N, McCrimmon DR, Feldman JL. Normal breathing requires preBotzinger complex neurokinin-1 receptor-expressing neurons. *Nature neuroscience*. 2001; 4:927–930. [PubMed: 11528424]
- Greer JJ, Smith JC, Feldman JL. Role of excitatory amino acids in the generation and transmission of respiratory drive in neonatal rat. *The Journal of physiology*. 1991; 437:727–749. [PubMed: 1653855]
- Janczewski WA, Tashima A, Hsu P, Cui Y, Feldman JL. Role of inhibition in respiratory pattern generation. *The Journal of neuroscience : the official journal of the Society for Neuroscience*. 2013; 33:5454–5465. [PubMed: 23536061]
- Johansson O, Hokfelt T, Elde RP. Immunohistochemical distribution of somatostatin-like immunoreactivity in the central nervous system of the adult rat. *Neuroscience*. 1984; 13:265–339. [PubMed: 6514182]
- Kam K, Worrell JW, Janczewski WA, Cui Y, Feldman JL. Distinct inspiratory rhythm and pattern generating mechanisms in the preBotzinger complex. *The Journal of neuroscience : the official journal of the Society for Neuroscience*. 2013a; 33:9235–9245. [PubMed: 23719793]
- Kam K, Worrell JW, Ventalon C, Emiliani V, Feldman JL. Emergence of population bursts from simultaneous activation of small subsets of preBotzinger complex inspiratory neurons. *The Journal of neuroscience : the official journal of the Society for Neuroscience*. 2013b; 33:3332–3338. [PubMed: 23426661]
- Koizumi H, Mosher B, Tariq MF, Zhang R, Koshiya N, Smith JC. Voltage-Dependent Rhythmogenic Property of Respiratory Pre-Bötzing Complex Glutamatergic, Dbx1-Derived, and Somatostatin-Expressing Neuron Populations Revealed by Graded Optogenetic Inhibition. *eNeuro*. 2016; 3 ENEURO.0081-0016.2016.
- Kottick A, Del Negro CA. Synaptic Depression Influences Inspiratory-Expiratory Phase Transition in Dbx1 Interneurons of the preBotzinger Complex in Neonatal Mice. *The Journal of neuroscience : the official journal of the Society for Neuroscience*. 2015; 35:11606–11611. [PubMed: 26290237]
- Kuna ST. Inhibition of inspiratory upper airway motoneuron activity by phasic volume feedback. *Journal of applied physiology (Bethesda, Md : 1985)*. 1986; 60:1373–1379.
- Li P, Janczewski WA, Yackle K, Kam K, Pagliardini S, Krasnow MA, Feldman JL. The peptidergic control circuit for sighing. *Nature*. 2016; 530:293–297. [PubMed: 26855425]
- Llona I, Eugenin J. Central actions of somatostatin in the generation and control of breathing. *Biological research*. 2005; 38:347–352. [PubMed: 16579516]
- Martel G, Dutar P, Epelbaum J, Viollet C. Somatostatinergic systems: an update on brain functions in normal and pathological aging. *Frontiers in endocrinology*. 2012; 3:154. [PubMed: 23230430]
- McKay LC, Janczewski WA, Feldman JL. Sleep-disordered breathing after targeted ablation of preBotzinger complex neurons. *Nature neuroscience*. 2005; 8:1142–1144. [PubMed: 16116455]
- Picardo MC, Weragalaarachchi KT, Akins VT, Del Negro CA. Physiological and morphological properties of Dbx1-derived respiratory neurons in the pre-Botzinger complex of neonatal mice. *The Journal of physiology*. 2013; 591:2687–2703. [PubMed: 23459755]
- Revill AL, Vann NC, Akins VT, Kottick A, Gray PA, Del Negro CA, Funk GD. Dbx1 precursor cells are a source of inspiratory XII premotoneurons. *eLife*. 2015; 4



- Schwarzacher SW, Rub U, Deller T. Neuroanatomical characteristics of the human pre-Botzinger complex and its involvement in neurodegenerative brainstem diseases. *Brain : a journal of neurology*. 2011; 134:24–35. [PubMed: 21115469]
- Sherman D, Worrell JW, Cui Y, Feldman JL. Optogenetic perturbation of preBotzinger complex inhibitory neurons modulates respiratory pattern. *Nature neuroscience*. 2015; 18:408–414. [PubMed: 25643296]
- Stornetta RL, Rosin DL, Wang H, Sevigny CP, Weston MC, Guyenet PG. A group of glutamatergic interneurons expressing high levels of both neurokinin-1 receptors and somatostatin identifies the region of the pre-Botzinger complex. *The Journal of comparative neurology*. 2003; 455:499–512. [PubMed: 12508323]
- Tan W, Janczewski WA, Yang P, Shao XM, Callaway EM, Feldman JL. Silencing preBotzinger complex somatostatin-expressing neurons induces persistent apnea in awake rat. *Nature neuroscience*. 2008; 11:538–540. [PubMed: 18391943]
- Tan W, Pagliardini S, Yang P, Janczewski WA, Feldman JL. Projections of preBotzinger complex neurons in adult rats. *The Journal of comparative neurology*. 2010; 518:1862–1878. [PubMed: 20235095]
- Tan W, Sherman D, Turesson J, Shao XM, Janczewski WA, Feldman JL. Reelin demarcates a subset of pre-Botzinger complex neurons in adult rat. *The Journal of comparative neurology*. 2012; 520:606–619. [PubMed: 21858819]
- Wallén-Mackenzie Å, Gezelius H, Thoby-Brisson M, Nygård A, Enjin A, Fujiyama F, Fortin G, Kullander K. Vesicular Glutamate Transporter 2 Is Required for Central Respiratory Rhythm Generation But Not for Locomotor Central Pattern Generation. *The Journal of Neuroscience*. 2006; 26:12294–12307. [PubMed: 17122055]
- Wang X, Hayes JA, Revill AL, Song H, Kottick A, Vann NC, LaMar MD, Picardo MC, Akins VT, Funk GD, et al. Laser ablation of Dbx1 neurons in the pre-Botzinger complex stops inspiratory rhythm and impairs output in neonatal mice. *eLife*. 2014; 3:e03427. [PubMed: 25027440]
- Wei XY, Zhao Y, Wong-Riley MT, Ju G, Liu YY. Synaptic relationship between somatostatin- and neurokinin-1 receptor-immunoreactive neurons in the pre-Botzinger complex of rats. *Journal of neurochemistry*. 2012; 122:923–933. [PubMed: 22765158]
- Winter SM, Fresemann J, Schnell C, Oku Y, Hirrlinger J, Hulsman S. Glycinergic interneurons are functionally integrated into the inspiratory network of mouse medullary slices. *Pflügers Archiv : European journal of physiology*. 2009; 458:459–469. [PubMed: 19238427]

**Highlights**

- Preinspiratory preBötC Dbx1<sup>+</sup> neurons are respiratory rhythmogenic.
- Inspiratory preBötC Dbx1<sup>+</sup> and SST<sup>+</sup> neurons shape motor output pattern.
- SST<sup>+</sup> neuron-mediated inhibitory pathways modulate respiratory activity.
- Postsynaptic inhibition broadens dynamic range and stabilizes breathing pattern.

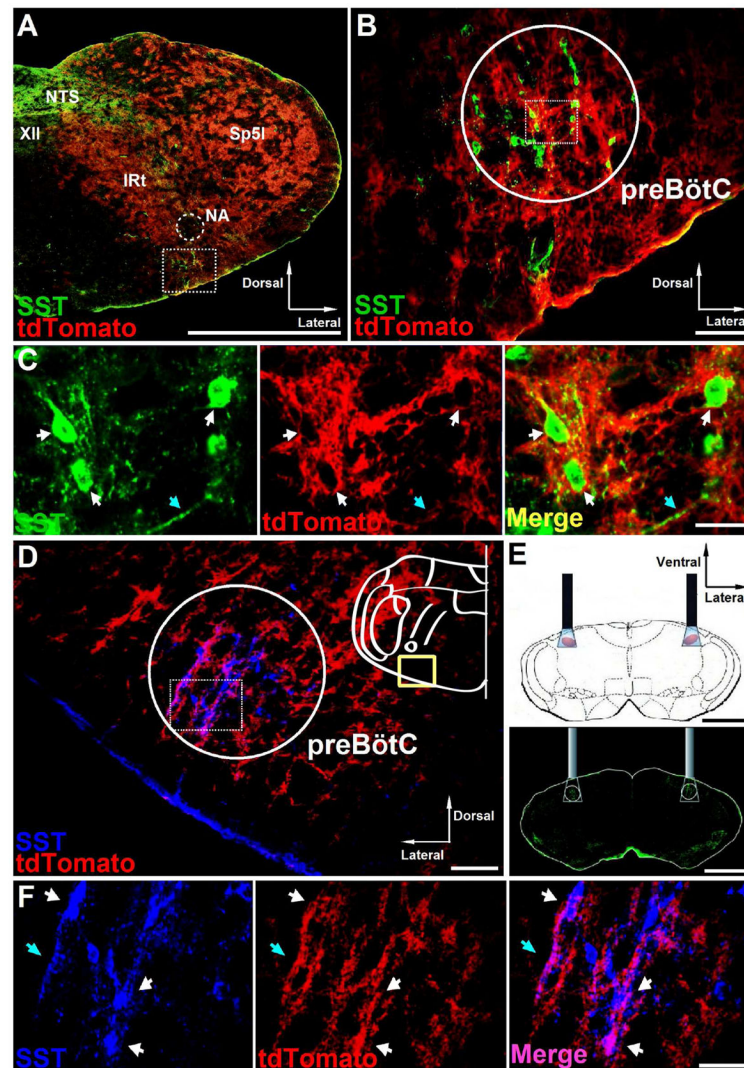


**Figure 1.**

ChR2 expression in preBötC neurons in transgenic mice. A, Distribution of Dbx1<sup>+</sup> neurons in coronal brainstem sections from adult Dbx1-ChR2 transgenic mice at the level of preBötC. The square segment showing preBötC area is expanded in B. Scale bar, 1 mm. NTS, nucleus of the solitary tract; XII, hypoglossal motor nucleus; NA, nucleus ambiguus; IRt, intermediate reticular nucleus; Sp5I, spinal trigeminal nucleus, interpolar part. B, tdTomato (red) in preBötC SST<sup>+</sup> neurons (green) of Dbx1-ChR2 transgenic mice. Scale bar, 100  $\mu$ m. C, High-magnification micrographs from the square segment in the circled area in B show single channel and overlay confocal micrographs of preBötC SST<sup>+</sup> neurons (green) with tdTomato fluorescence (red). White arrows point to neuron cell bodies. Blue arrows point to neuron fibers. Scale bar, 20  $\mu$ m. D, Coronal section from adult SST-ChR2 transgenic mice at the level of preBötC showing tdTomato (red) overlaps with SST<sup>+</sup> neurons (blue) in the preBötC; scale bar, 100  $\mu$ m. E, Schematic (top) and coronal section stained for SST (green, bottom) depicting bilateral placement of optical cannulae targeting preBötC. Scale bar, 1 mm. F, High-magnification micrographs from the square segment in the circled area in

D show single channel and overlay confocal micrographs of preBötC SST<sup>+</sup> neurons (blue) with tdTomato fluorescence (red). White arrows point to neuron cell bodies. Blue arrows point to neuron fibers. Scale bar, 50  $\mu$ m.

Author Manuscript

Author Manuscript

Author Manuscript

Author Manuscript

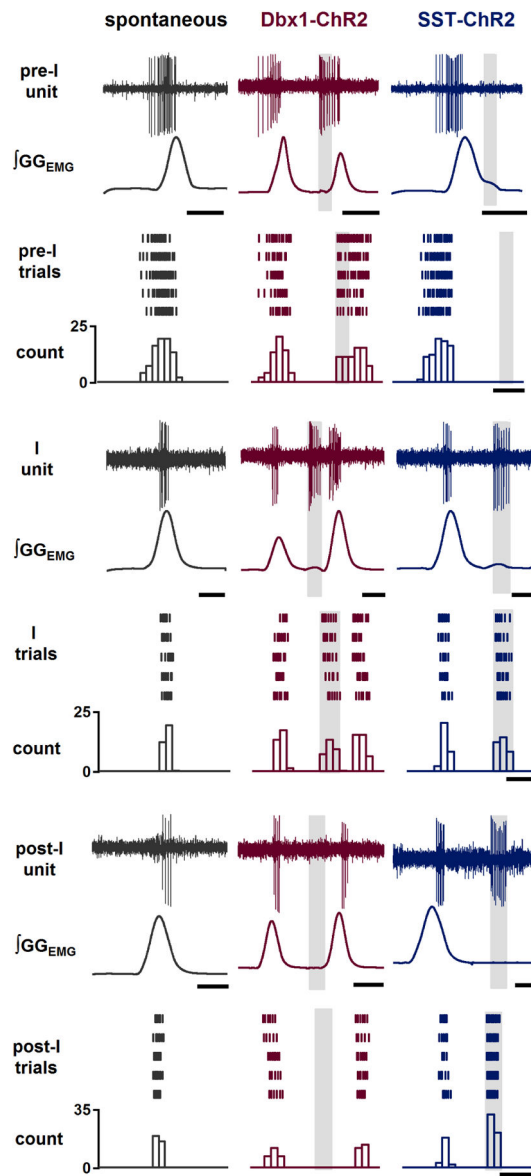


**Figure 2.** preBötC respiratory-modulated neuron firing patterns at baseline and in response to preBötC photostimulation in Dbx1-ChR2 and SST-ChR2 mice. Left column (black): Representative traces of  $\int GG_{EMG}$  and preBötC respiratory-modulated neurons with various firing patterns (pre-I, top, scale bar, 0.4 s; I, middle, scale bar, 0.2 s; and post-I, bottom, scale bar, 0.2 s) recorded in mice *in vivo*. Middle (red) and Right (blue) column: Representative traces of  $\int GG_{EMG}$  and preBötC respiratory-modulated neuron (pre-I, top, scale bars, 0.4 s; I, middle, scale bars, 0.2 s; and post-I, bottom, scale bars, 0.2 s) firing patterns at baseline and in response to 7 mW light illumination (gray box) targeted to preBötC in Dbx1-ChR2 (red) and SST-ChR2 (blue) mice. Below traces are raster plots and cumulative histograms representing action potentials of preBötC respiratory-modulated neurons (scale bars, 0.25 s) during

baseline (left, black) and light-evoked (7 mW, gray box) bursts in Dbx1-ChR2 (middle, red) and SST-ChR2 (right, blue) mice.

Author Manuscript

Author Manuscript

Author Manuscript

Author Manuscript



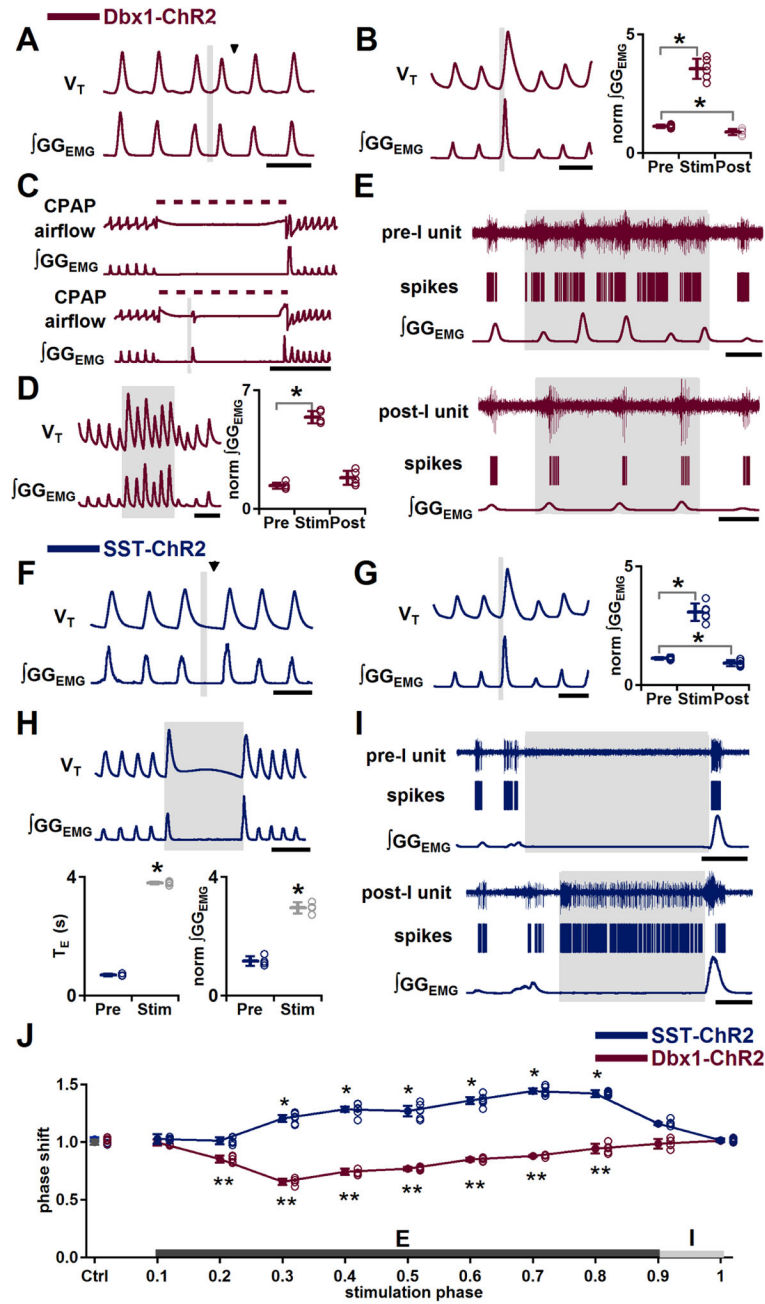


**Figure 3.** Effects of bilateral preBötC photostimulation on burst timing and motor output pattern in Dbx1-ChR2 and SST-ChR2 mice. (A–E) In Dbx1-ChR2 mice, bilateral preBötC photostimulation is excitatory. A, Ectopic inspiratory burst induced by bilateral preBötC SPP during midexpiration. Black arrowhead indicates expected onset of inspiratory burst following photostimulation. Scale bar, 1 s. B, Left: Augmented inspiratory bursts induced by bilateral preBötC SPP in early inspiration. Scale bar, 1 s. Right: Bilateral preBötC SPP effects on normalized (norm)  $\int GG_{EMG}$  prestimulation (Pre), during stimulation (Stim) and poststimulation (Post) (\*,  $P < 0.05$ ;  $n = 6$ ). C, During an inflation-induced apnea (top), bilateral

preBötC SPP broke apnea for pulse duration (bottom). Dotted line represents CPAP (8 cm H<sub>2</sub>O). Scale bar, 5 s. D, Left: Bilateral preBötC LPP produced augmented inspiratory bursts. Scale bar, 2 s. Right: Bilateral preBötC LPP effects on norm  $\int GG_{EMG}$  Pre, during Stim and Post (\*, P<0.05; n=5). E, Firing patterns of preinspiratory (pre-I; top) and postinspiratory (post-I; bottom) preBötC neurons in response to bilateral preBötC LPP in Dbx1-ChR2 mice. Scale bar, 1 s. (F–I) In SST-ChR2 mice, bilateral preBötC photostimulation evoked phase-dependent excitatory or inhibitory responses. F, Bilateral preBötC SPP during midexpiration depressed inspiratory motor output or lengthened expiratory duration. Black arrowhead indicates the expected onset of inspiratory burst following photostimulation. Scale bar, 1 s. G, Left: Augmented inspiratory bursts induced by bilateral preBötC SPP in early inspiration. Scale bar, 1 s. Right: Bilateral preBötC SPP effects on norm  $\int GG_{EMG}$  Pre, during Stim and Post (\*, P<0.05; n=6). H, Top: Apneas produced by bilateral preBötC LPP. Scale bar, 2 s. Bottom: Left: Duration of bilateral preBötC LPP-induced apnea compared to  $T_E$  of the previous cycle (\*, P<0.05; n=4). Right: Amplitude of the  $GG_{EMG}$  burst induced by bilateral preBötC LPP compared to  $\int GG_{EMG}$  of previous cycle (\*, P<0.05; n=4). I, Firing patterns of preinspiratory (pre-I; top) and postinspiratory (post-I; bottom) preBötC neurons in response to bilateral preBötC LPP in SST-ChR2 mice. Scale bar, 1 s. J, Phase response curves show that bilateral preBötC SPP in SST-ChR2 mice (blue; n=6) led to phase delays and bilateral preBötC SPP in Dbx1-ChR2 mice (red; n=5) led to phase advances. \*, \*\* comparisons versus control phase shift (Ctrl), P<0.05. Error bars represent mean±SD.

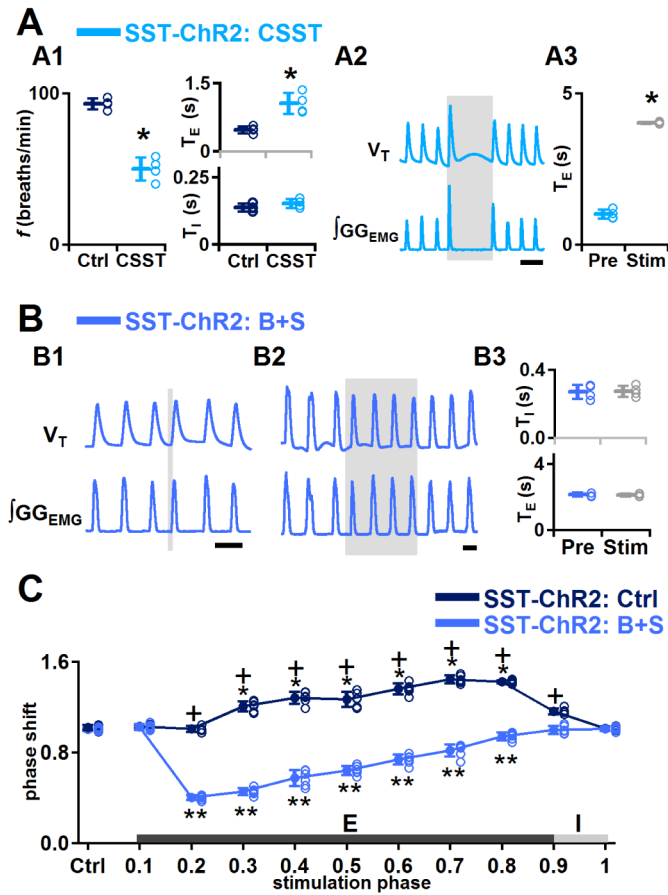


**Figure 4.**

Effects of bilateral preBötC photostimulation in SST-ChR2 mice after pharmacological injection of SST receptor antagonist CSST or bicuculline and strychnine (B+S). **A**, In SST-ChR2 mice, SST antagonism did not eliminate apnea induced by bilateral preBötC LPP. **A1**:  $f$ ,  $T_I$ , and  $T_E$  measured before (Ctrl) and after (CSST) administration of CSST (\*,  $P < 0.05$ ;  $n = 4$ ). **A2**: Bilateral preBötC injection of CSST did not eliminate apnea induced by bilateral preBötC LPP. Scale bar, 2 s. **A3**: Duration of bilateral preBötC LPP-induced apnea after administration of CSST compared to  $T_E$  of previous cycle (\*,  $P < 0.05$ ;  $n = 4$ ). **B**, In SST-ChR2 mice, B+S eliminated the bilateral preBötC LPP-induced apnea and SPP-induced prolongation in expiratory duration. **B1**: Bilateral preBötC SPP during midexpiration in B+S in SST-ChR2 mice triggered an ectopic inspiratory burst. Scale bar, 2 s. **B2**: Bilateral preBötC LPP in B+S in SST-ChR2 mice no longer produced apnea. Scale bar, 2 s. **B3**: Bilateral preBötC LPP in B+S in SST-ChR2 mice did not change  $T_I$  or  $T_E$ . **C**, Phase response curves show bilateral preBötC SPP in SST-ChR2 mice before block of inhibition (SST-ChR2: Ctrl, dark blue) led to phase delays that became phase advances after block of inhibition (SST-ChR2: B+S, light blue). \*, \*\* comparisons versus control phase shift (Ctrl),  $P < 0.05$ ; +, comparisons of the phase shift before and after B+S injection,  $P < 0.05$ . Error bars represent mean  $\pm$  SD.

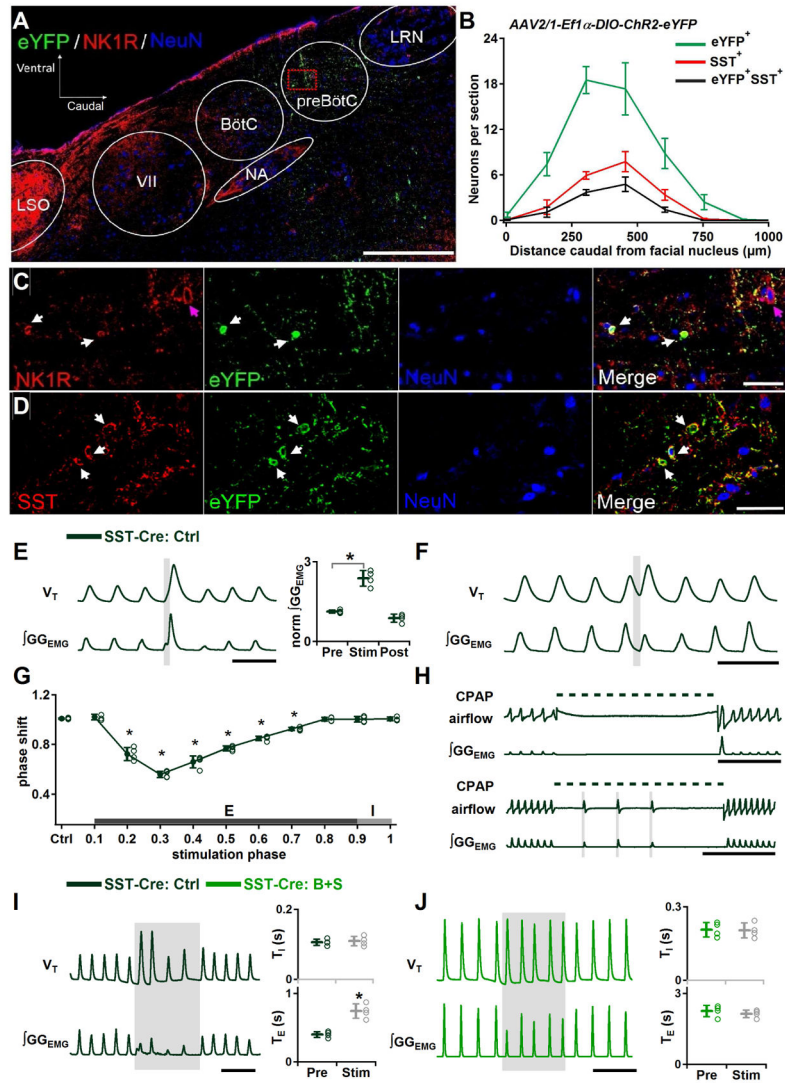


**Figure 5.**

Excitatory role for SST<sup>+</sup> glutamatergic preBötC neurons and a SST<sup>+</sup> neuron-mediated inhibitory pathway within preBötC. (A–D) Cre dependent Chr2 expression targeted to preBötC SST neurons. A, Representative confocal mosaic micrograph of sagittal brainstem section of SST-Cre mouse showing the extent of eYFP<sup>+</sup>, SST<sup>+</sup> and NK1R<sup>+</sup> neurons 4 weeks after injection of AAV2/1-Ef1 $\alpha$ -DIO-ChR2-eYFP into preBötC. Scale bar, 500  $\mu$ m. VII, facial nucleus; BötC, Bötzing Complex; NA, nucleus ambiguus; LRN, lateral reticular nucleus; LSO, lateral superior olive. B, Rostrocaudal distribution of eYFP (green), marking location of neurons expressing Chr2 (n = 4) and SST<sup>+</sup> (red) neurons relative to caudal boundary of facial nucleus. C, High-magnification single channel and overlay confocal micrographs of square in circled area demarking the preBötC in A show small fusiform NK1R<sup>+</sup> neurons (red, white arrows) were immunoreactive for eYFP (green). Large NK1R<sup>+</sup> neurons (red, purple arrows) were not colocalized with eYFP immunoreactivity. Section also labeled for NeuN (blue) immunoreactivity. Scale bar, 50  $\mu$ m. D, High-magnification micrograph showing colocalization (yellow) of Chr2-eYFP (green) and preBötC SST<sup>+</sup>

neurons (red) in ChR2-transfected SST-Cre mice. Section also labeled for NeuN (blue) immunoreactivity. Scale bar, 50  $\mu\text{m}$ . (E–H) Excitatory effect elicited by bilateral preBötC SPP in ChR2-transfected SST-Cre mice. E, Left: Augmented inspiratory bursts induced by bilateral preBötC SPP in early inspiration. Scale bar, 1 s. Right: Bilateral preBötC SPP in early inspiration effects on normalized ( $\text{norm}$ )  $\int \text{GG}_{\text{EMG}}$  prestimulation (Pre), during stimulation (Stim) and poststimulation (Post) (\*,  $P < 0.05$ ;  $n = 4$ ). F, Ectopic inspiratory burst elicited by bilateral preBötC SPP during midexpiration in ChR2-transfected SST-Cre mice. Scale bar, 1 s. G, Phase response curve shows bilateral preBötC SPP in ChR2-transfected SST-Cre mice led to phase advances. \*, comparisons versus control phase shift (Ctrl),  $P < 0.05$ . H, Each of three bilateral preBötC SPPs in ChR2-transfected SST-Cre mice induced a breath during an inflation-induced apnea. Dotted line represents CPAP (8 cm  $\text{H}_2\text{O}$ ). Scale bar, 5 s. (I–J) The remaining inhibitory effect in virus transfected SST-Cre mice was mediated by GABA and/or glycine. I, Left: Bilateral preBötC LPP in ChR2 transfected SST-Cre mice did not induce apnea but slowed down breathing frequency. Scale bar, 2 s. Right:  $T_I$  (top) and  $T_E$  (bottom) measured before (Pre) and during bilateral preBötC LPP (Stim) (\*,  $P < 0.05$ ;  $n = 4$ ). J, Left: Bilateral preBötC LPP no longer produced prolongation in  $T_E$  after blocking inhibition within preBötC in ChR2 transfected SST-Cre mice. Scale bar, 5 s. Right:  $T_I$  (top) and  $T_E$  (bottom) measured Pre and during Stim in B+S. Error bars represent mean  $\pm$ SD.

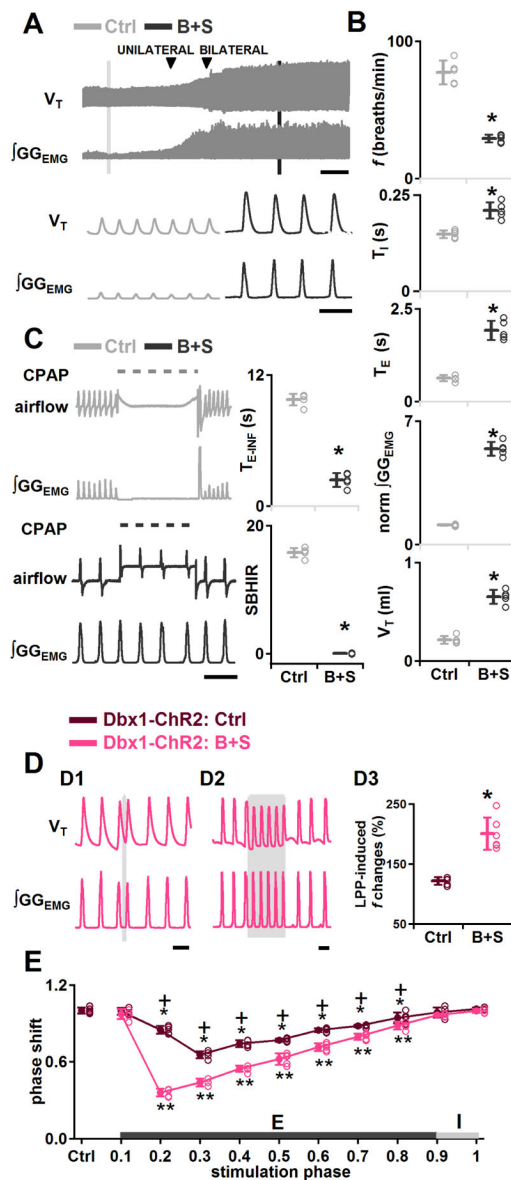


**Figure 6.** Effects of GABA and glycine antagonism in preBötC on rhythmogenesis. (A–C) In anesthetized wild type mice. A, Representative  $V_T$  and  $\int GG_{EMG}$  (top; scale bar, 2 min) and expanded (bottom; scale bar, 2 s) traces show the effects of bilateral preBötC B+S injection on  $\int GG_{EMG}$  and  $V_T$ . B,  $f$ ,  $T_I$ ,  $T_E$ , Normalized (norm)  $\int GG_{EMG}$ ,  $V_T$ , measured in control (vagus intact) (Ctrl), and after administration of B+S (B+S) (\*,  $P < 0.05$ ;  $n = 5$ ). C, Left: Lung inflation induced apnea in control (top) but was suppressed by B+S (bottom). Dotted line represents CPAP (8 cm H<sub>2</sub>O). Scale bar, 5 s. Right:  $T_{E-INF}$  and the SBHIR measured in control (vagus intact) (Ctrl) and after B+S injection (B+S) (\*,  $P < 0.05$ ;  $n = 5$ ). D, Enhanced excitatory effects on burst timing elicited by bilateral preBötC photostimulation in Dbx1-ChR2 mice after block of fast synaptic inhibition. D1: Ectopic inspiratory burst elicited by bilateral preBötC SPP in Dbx1-ChR2 mice during midexpiration after B+S injection. Scale



bar, 2 s. D2: Bilateral preBötC LPP in Dbx1-ChR2 mice in B+S shows enhanced excitatory effect on  $f$ . Scale bar, 2 s. D3: Bilateral preBötC LPP in Dbx1-ChR2 mice after block of inhibition (B+S) produced a greater increase in  $f$ (\* ,  $P<0.05$ ;  $n=5$ ). E, Phase response curves show bilateral preBötC SPP in Dbx1-ChR2 mice during mid or late expiration after block of inhibition produced a stronger phase-resetting (pink). \*, \*\* comparisons versus control phase shift,  $P<0.05$ ; +, comparisons of the phase shift before and after B+S injection,  $P<0.05$ . Error bars represent mean $\pm$ SD.

Author Manuscript

Author Manuscript

Author Manuscript

Author Manuscript

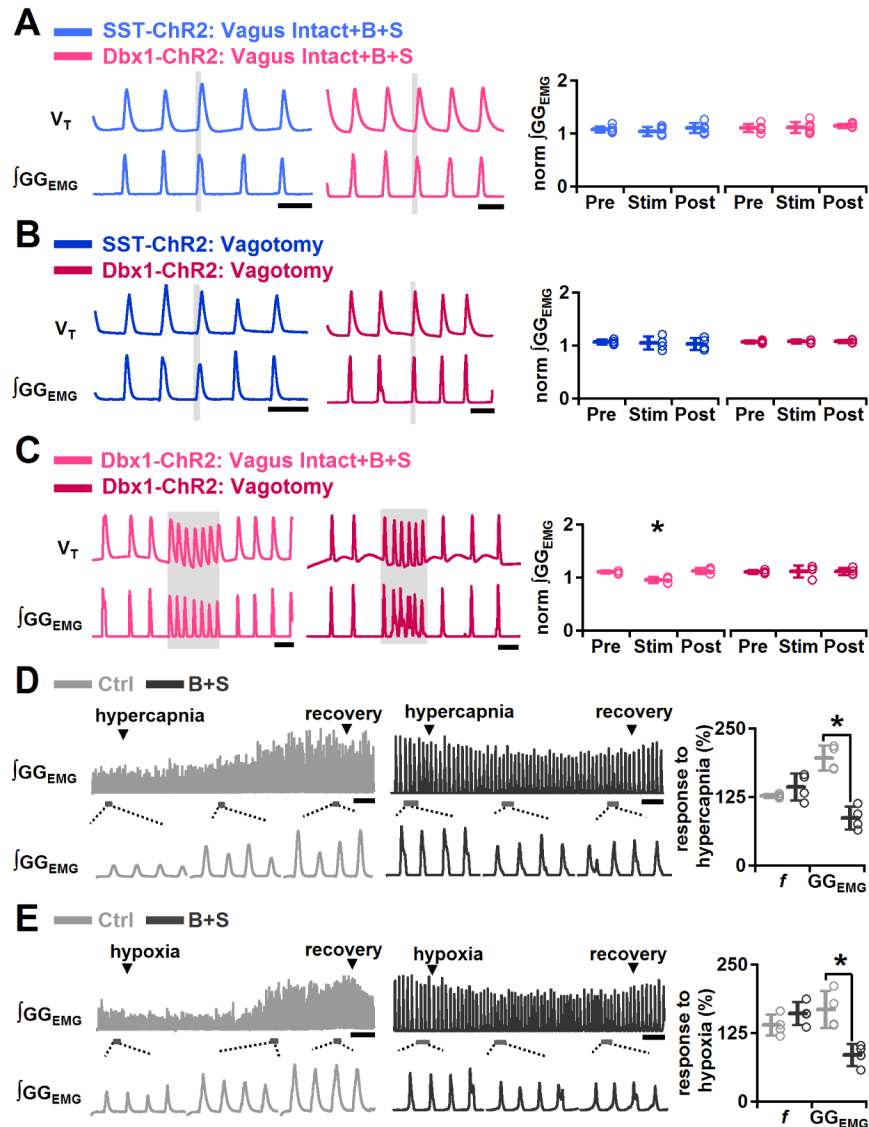


**Figure 7.**

GABA and glycine antagonism in preBötC maximized inspiratory burst amplitude. A, Bilateral preBötC SPP in Dbx1-ChR2 and SST-ChR2 mice were unable to increase  $\int GG_{EMG}$  burst amplitude further after B+S injection. Left: Bilateral preBötC SPP in early inspiration in vagus intact Dbx1-ChR2 (pink) and SST-ChR2 (light blue) mice after B+S injection did not increase  $\int GG_{EMG}$  burst amplitude. Scale bar, 2 s. Right: In SST-ChR2 (light blue) and Dbx1-ChR2 (pink) mice after B+S injection, bilateral preBötC SPP effects on normalized (norm)  $\int GG_{EMG}$  prestimulation (Pre), during stimulation (Stim) and poststimulation (Post) ( $n=5$ ). B, Bilateral preBötC SPP in Dbx1-ChR2 and SST-ChR2 mice were unable to increase  $\int GG_{EMG}$  burst amplitude further after vagotomy. Left: After vagotomy, bilateral preBötC SPP in early inspiration in SST-ChR2 (dark blue) and Dbx1-ChR2 (red) mice did not increase  $\int GG_{EMG}$  burst amplitude. Scale bar, 2 s. Right: In SST-ChR2 (dark blue) and Dbx1-ChR2 (red) mice after vagotomy, bilateral preBötC SPP effects on normalized (norm)  $\int GG_{EMG}$  Pre, during Stim and Post ( $n=4$ ). C, Bilateral preBötC LPP in Dbx1-ChR2 mice

was unable to increase  $GG_{EMG}$  burst amplitude further in B+S or after vagotomy. Left: In Dbx1-ChR2 mice in B+S (pink) or after vagotomy (red), bilateral preBötC LPP did not increase burst amplitude. Scale bar, 2 s. Right: In Dbx1-ChR2 mice in B+S (pink) (\*,  $P < 0.05$ ;  $n = 5$ ) or after vagotomy (red) ( $n = 4$ ), bilateral preBötC LPP effects on norm  $\int GG_{EMG}$  Pre, during Stim and Post. (D–E) Responses to increased chemical drive in wild type mice before and after block of inhibition within the preBötC. D, Left: Representative  $GG_{EMG}$  (top) and expanded trace (bottom) of the responses to hypercapnia before (light gray) and in (dark gray) B+S show that hypercapnic challenges after block of inhibition did not further increase  $GG_{EMG}$  burst amplitude. Scale bar, 10 s. Right: Increase in  $GG_{EMG}$  burst amplitude ( $GG_{EMG}$ ) and  $f$  before (light gray) and after B+S injection (dark gray) in response to hypercapnia (\*,  $P < 0.05$ ;  $n = 4$ ). E, Left: Representative  $GG_{EMG}$  (top) and expanded trace (bottom) of the responses to hypoxia before (light gray) and after (dark gray) B+S show that hypoxic challenges after block of inhibition did not further increase  $GG_{EMG}$  burst amplitude. Scale bar, 10 s. Right: Increase in  $GG_{EMG}$  and  $f$  before (light gray) and after B+S injection (dark gray) in response to hypoxia (\*,  $P < 0.05$ ;  $n = 4$ ). Error bars represent  $\text{mean} \pm \text{SD}$ .

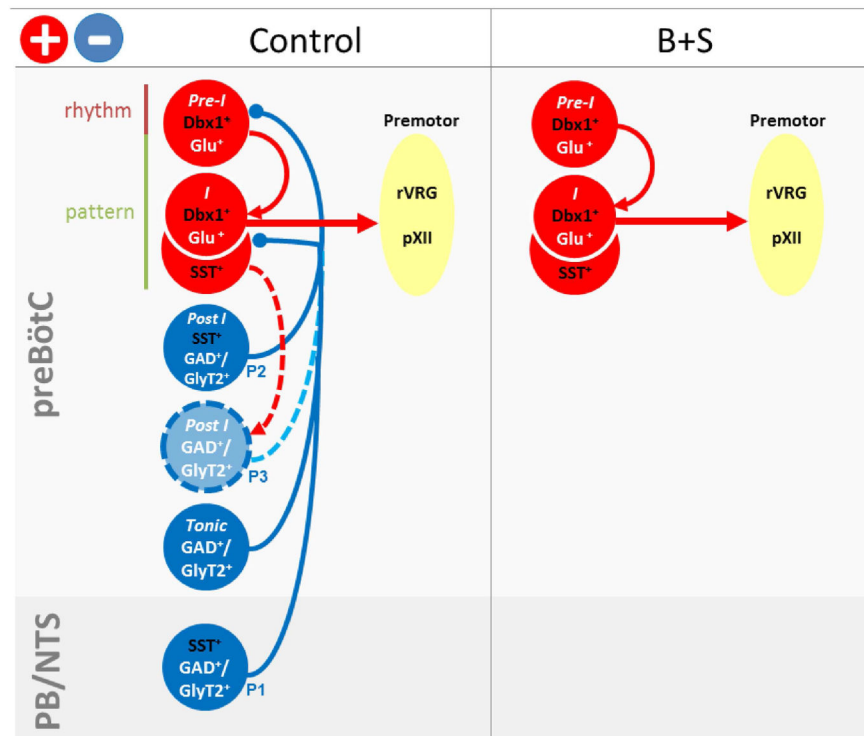


**Figure 8.**

Functional roles of preBötC subpopulations in respiratory rhythm and pattern generation. Model shows map of interconnections of respiratory-related neuronal subpopulations in control (left) or after administration of B+S into preBötC (right). Data supporting this scheme are summarized in Figure S4. We postulate that preBötC burst (pattern) generation is a two-stage process consisting of a low amplitude rhythmogenic preinspiratory component (Pre-I) and a high amplitude pattern generating inspiratory burst (I) (Kam et al., 2013a, Feldman and Kam, 2015). Preinspiratory  $\text{Dbx1}^+$  neurons (Pre-I  $\text{Dbx1}^+\text{Glu}^+$ ) serve as the rhythmogenic preinspiratory component that determines onset of inspiratory bursts. Inspiratory  $\text{SST}^+$  neurons (I  $\text{SST}^+\text{Glu}^+$ ) and inspiratory  $\text{Dbx1}^+$  neurons (I  $\text{Dbx1}^+\text{Glu}^+$ ) are triggered by Pre-I  $\text{Dbx1}^+$  neurons to generate the inspiratory burst that is transmitted to inspiratory premotoneurons, that in turn project to motoneurons innervating inspiratory muscles, e.g., diaphragm; this serves as part of the pattern-generating process. Left: Rhythmogenic and pattern-generating neurons receive inhibitory inputs from various GABAergic and/or glycinergic neurons that could stabilize the rhythm and increase dynamic range of inspiratory output. Beside  $\text{SST}^+$ -afferents from nucleus of the solitary tract (NTS) and parabrachial nuclei (PB), both outside the preBötC ( $\text{SST}^+\text{GAD}^+\text{GlyT2}^+$ , P1), inhibitory effects induced by  $\text{SST}^+$  neuron photoactivation could result from unidentified GABAergic and/or glycinergic preBötC  $\text{SST}^+$  neurons (Post-I  $\text{SST}^+\text{GAD}^+\text{GlyT2}^+$ , P2), or non- $\text{SST}^+$  GABAergic and/or glycinergic post-I neurons (Post-I  $\text{GAD}^+\text{GlyT2}^+$ , P3) downstream from glutamatergic  $\text{SST}^+$  neurons (I  $\text{SST}^+\text{Glu}^+$ ) within preBötC. Right: After inhibitory blockade with administration of B+S into the preBötC, only excitatory preBötC neurons remain, with consequential effects on the responses to photostimulation of  $\text{SST}^+$  neurons.